ACS APPLIED MATERIALS & INTERFACES

Research Article

www.acsami.org

Sulfur- and Nitrogen-Doped, Ferrocene-Derived Mesoporous Carbons with Efficient Electrochemical Reduction of Oxygen

Jiaoxing Xu,[†,‡] Yi Zhao,[†,‡] Cai Shen,[§] and Lunhui Guan*[,†,‡]

[†]State Key Structural Chemistry Laboratory and Fujian Institute of Research on the Structure of Matter, Chinese Academy of Sciences, Fuzhou, Fujian 350002, China

[‡]Key Laboratory of Design and Assembly of Functional Nanostructures, Chinese Academy of Sciences, Fuzhou, Fujian 350002, China

[§]Ningbo Institute of Materials Technology & Engineering (NIMTE), Chinese Academy of Sciences, Ningbo 615201, China

Supporting Information

ABSTRACT: Development of inexpensive and sustainable cathode catalysts that can efficiently catalyze the oxygen reduction reaction (ORR) is of significance in practical application of fuel cells. Herein we report the synthesis of sulfur and nitrogen dual-doped, ordered mesoporous carbon (SN-OMCs), which shows outstanding ORR electrocatalytic properties. The material was synthesized from a surface-templating process of ferrocene within the channel walls of SBA-15 mesoporous silica by carbonization, followed by in situ heteroatomic doping with sulfur- and nitrogen-containing vapors. After etching away the metal and silica template, the resulting material features distinctive bimodal mesoporous carbon frameworks with high nitrogen Brunauer–Emmett–Teller specific surface area (of up to ~1100 m^2/g) and uniform distribution of sulfur and nitrogen dopants. When employed as a noble-metal-free electrocatalyst for the ORR, such SN-OMC shows a remarkable electrocatalytic activity; improved durability and better resistance toward methanol crossover in oxygen reduction can be observed. More importantly, it performs a low onset voltage and an efficient nearly complete four-electron ORR process very similar to the observations in commercial 20 wt % Pt/C catalyst. In addition, we also found that the textural mesostructure of the catalyst has superseded the chemically bonded dopants to be the key factor in controlling the ORR performance.

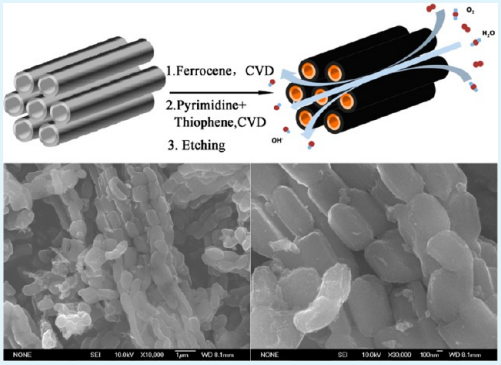

KEYWORDS: *fuel cells, electrocatalyst, ORR, non-precious-metal catalyst, doped carbons, mesoporous*

1. INTRODUCTION

Slow oxygen reduction reaction (ORR) kinetics and high cost of Pt catalysts at the cathode are major barriers against development of commercially available fuel cells.[1,2] Extensive efforts have been devoted to either reducing the amount of Pt-based catalyst or replacing them.[3−7] Pt-free and non-precious-metal catalysts (NPMCs), such as heteroatom-doped (N-doped) carbon materials, have been regarded as the most potential substitute due to their high efficiency, durability, and low production cost.[6,8−10] For instance, vertically aligned carbon nanotube arrays doped with nitrogen showed pronounced ORR electrocatalytic activity, stability, and tolerance toward poisoning in alkaline media.[8] The enhanced electrocatalytic activity is probably attributed to the new catalytic sites created via substitutionally doping with a heteroatom, which breaks the electroneutrality of the carbon plane on the carbon nanotubes, though the debate on the active sites is still going on.[10−12] Other elements beyond N (e.g., B,[10] P,[13] S, Se,[14] and I[15]) were also introduced into the carbon framework for generating effective ORR electrocatalysts. Although these "active" element-doped carbon materials can enhance the ORR efficiency, they hardly supersede the performance of the commercial Pt/C catalyst especially under the operating conditions of fuel cells. To address this issue, some researchers proposed that doping carbons with nitrogen and other heteroatoms[2,7,16] can provide further space for performance optimization. Recent studies revealed that mesoporous graphene[17] or few-layered graphene oxide[18] gave rise to considerable enhanced ORR electrocatalytic activity upon sulfur and nitrogen doping, beneficial from the increased number of dopants and the synergistic effects between the dopants. Although dual-doped graphene materials have better performance than N-doped materials, the ORR catalytic activities are still far from satisfactory, partially because of the relatively low surface utilization (<500 $m^2\ g^{-1}$) from the irreversible multilayer stacking and randomly formed inaccessible narrow pores.[19] Thus, a uniform structure with relatively large surface area and regular pores is more preferable[20,21] to enhance the catalytic activity.

Received: September 10, 2013
Accepted: November 18, 2013
Published: November 18, 2013

Herein we report a template synthesis of sulfur and nitrogen dual-doped, ordered mesoporous carbons (SN-OMCs) with outstanding ORR electrocatalytic properties. The SN-OMCs were synthesized from a surface-templating process of ferrocene within the pores of SBA-15 mesoporous silica by carbonization, followed by in situ heteroatomic doping with thiophene and pyrimidine as S and N precursors, and finally etching away the silica framework and Fe catalyst, as illustrated in Scheme 1. The resulting material features a unique bimodal porous framework, with a high nitrogen Brunauer–Emmett–Teller (BET) specific surface area up to of 1100 m^2/g. When employed as a noble-metal-free electrocatalyst for the ORR in alkaline media, such SN-OMC shows remarkable electrocatalytic activity, enhanced durability, and better resistance to crossover effect in oxygen reduction with respect to the commercial Pt/C catalyst. Particularly, it demonstrates a small overpotential and nearly 100% of four-electron ORR processes that are very similar to the observations in the commercial 20 wt % Pt/C catalyst. Such excellent electrochemical performance, until now, has rarely been observed for non-precious-metal catalysts.[2,22]

Scheme 1. Schematical Illustration of the Template Fabrication Process of SN-OMCs[a]

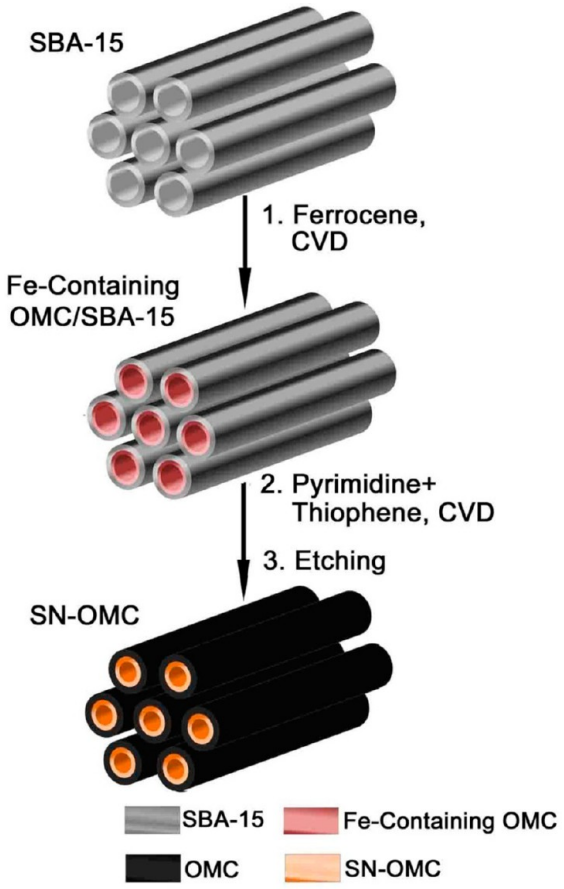

[a]It involved (1) a surface-templating process of ferrocene within the channel walls of SBA-15 mesoporous silica by carbonization, followed by (2) a heteroatomic doping with thiophene and pyrimidine as sulfur and nitrogen precursors, and (3) finally etching away the metal and mesoporous silica framework.

2. EXPERIMENTAL SECTION

2.1. Material Preparation. *2.1.1. Reagents.* The precursors of pyrimidine (98 %) and thiophene (99 %) were purchased from Aladdin (Shanghai, China) and Alfa Aesar (Tianjin, China), respectively. Ferrocene (chemical grade) and tetraethyl orthosilicate (TEOS, analytic grade) were purchased from Sinopharm Chemical Reagent Co., Ltd. (Shanghai, China). Pluronic P123 (EO20-PO70EO20, M_w ~5800) was purchased from Sigma Aldrich (Germany). All reagents were used without further purification.

2.1.2. Fabrication of Mesoporous Silica Template. SBA-15 silica template was prepared according to the previous reported method.[23] Typically, 4 g of Pluronic P123 was dissolved in 150 mL of 1.6 M HCl at 38 °C, then 8.5 g of TEOS was added to the transparent solution with vigorous stirring for 8 min and the mixture was left under vigorous stirring at the same temperature for 24 h. The mixture was subsequently treated at 100 °C for another 24 h in an autoclave. The as-synthesized SBA-15 silica was collected by filtration, washed with distilled water, dried at 80 °C overnight, and finally calcined at 550 °C for 5 h in air to get the final product.

2.1.3. Template Fabrication of Mesoporous SN-OMCs. The templating method to fabricate the mesoporous SN-OMC is illustrated in Scheme 1. The synthetic details involve the formation of ordered mesoporous carbon framework (OMC) under chemical vapor deposition (CVD) conditions and the subsequent in situ heteroatomic doping. First, to prepare the OMC framework, 0.15 g of SBA-15 mesoporous silica was put at the central part of vertical quartz tube in a furnace. Close to the furnace, a glass tube with an open glass bulb at the middle position was used to hold 0.8 g of ferrocene, which links the quartz tube with a reducer union. The whole reaction system is schematically shown in Supporting Information (Scheme S1). Under a flow rate of 80 mL min^{-1} of N_2, the temperature of the furnace was increased to 500 °C. Afterward, the temperature of the glass bulb was also heated to 120 °C by a heating tape, and the sublimation vapor of ferrocene was carried by N_2 to pass through the silica SBA-15 for surface-templating growth of OMC. Second, with the controlled formation of OMC within the silica SBA-15 template, the furnace temperature was further elevated toward 700 °C. Then, 3 mL of the steam of thiophene and pyrimidine mixtures (with an optimum ratio of $V_{thiophene}/V_{pyrimidine}$ = 1:4)[18] was carried by N_2 flowing gas to pass through the silica SBA-15-supported OMC for heteroatomic doping, with simultaneous deposition of sulfur- and nitrogen-containing carbons. Thereafter, the reaction system cooled naturally to ambient condition. The product was collected and sequentially refluxed in 6 M NaOH and 6 M HCl aqueous solution at 50 °C for 24 h to remove the silica template and Fe catalysts and finally washed with deionized water and dried at 80 °C overnight.

To optimize CVD conditions for acquiring the best ORR electrocatalytic activity, the intermediate ferrocene-derived OMC framework, which replicated from the mesoporous SBA-15 silica template, was adjusted by varying the deposition time from 20 min, 4 h, and 8 h. The corresponding SN-OMCs are designated as SN-OMC-1/3, SN-OMC-4, and SN-OMC-8 orderly. Prolonging the CVD growth of OMC for enough time (16 h) led to the complete filling of the inner pores of SBA-15 mesoporous silica, and the resultant single-channel SN-OMC was denoted as SN-OMC-16. To distinguish the respective contribution of doped sulfur atoms and nitrogen atoms to the improved ORR electrocatalytic activity, the mono-N-doped OMC (N-OMC) and S-doped OMC (S-OMC) samples were synthesized at the optimized CVD conditions (4 h) and with the presence of pyrimidine and thiophene, respectively. To explore the role of the mesoporous SBA-15 silica template, the sulfur- and nitrogen-co-doped oligoporous carbon (SN-C) as a reference sample was also prepared in the absence of the silica template.

2.2. Material Characterizations. The structure and morphology of the SN-OMCs were characterized by small-angle X-ray scattering (SAXS, X'Pert Pro MPD), scanning electron microscopy (SEM, JSM-6700F), and scanning transmission electron microscopy (STEM, FEI Tecnai G2 F20) equipped with energy-dispersive X-ray spectroscopy (EDS). X-ray photoelectron spectroscopic (XPS) measurements were

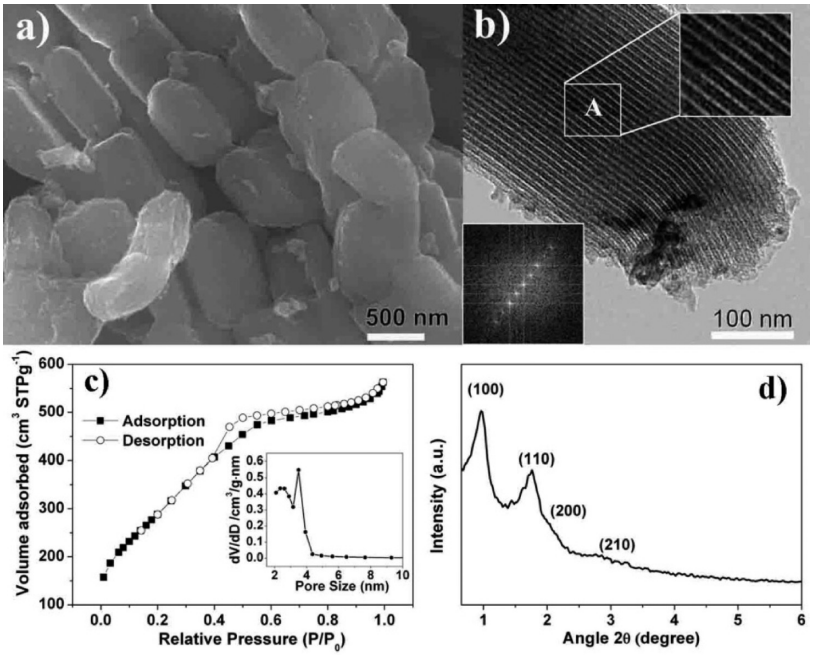

Figure 1. (a) SEM and (b) TEM images of a typical SN-OMC-4 sample; inset in (b) shows the corresponding fast Fourier transforms of the patterns; (c) N_2-sorption isotherm; the inset is the pore-size distribution, derived from the desorption branch of the isotherm and the Barrett–Joyner–Halenda formula; and (d) small-angle X-ray scattering pattern.

performed on a VG Scientific ESCALAB MK II using Al Kα radiation (1486.71 eV) and the C1s peak at 284.5 eV as an internal standard. The nitrogen adsorption/desorption data were recorded at the liquid nitrogen temperature (77 K) using a Micromeritics ASAP 2020 M appartus. Before the measurements, the samples were evacuated for 10 h at 200 °C. The specific surface area was calculated using the BET equation.

2.3. Electrochemical Test. Electrochemical measurements were conducted on an electrochemical workstation (CHI 760D, CH Instruments, Inc., Shanghai, China) coupled with a PINE rotating disk electrode (RDE) system (from Pine Instruments Co. Ltd. USA). A standard three-electrode electrochemical system equipped with gas flow system was employed. The procedure of the preparation of the electrode was similar to that in ref 18. The catalyst (5.0 mg), isopropyl alcohol (0.95 mL), and Nafion (50.0 μL, DuPont Corp., 5 wt %) were mixed and blended using an ultrasonic bath to obtain a homogeneous ink. The ink (12 μL) was pipetted onto a clean glassy carbon electrode (GCE) surface with a catalyst loading of 0.306 mg cm^{-2} to yield a GCE modified with a thin film of the catalyst, and the electrode was allowed to dry at room temperature for 30 min in a desiccator before measurement. For comparison, GCEs coated with Pt/C (20 wt % Pt on Vulcan XC-72, purchased from Alfa Aesar) were also fabricated using the same procedure. The ORR performance of the catalysts was studied by cyclic voltammogram (CV) and linear sweep voltammogram (LSV) measurements in an aqueous solution of 0.1 M NaOH. CVs were measured at a scan rate of 50 mV/s. LSVs were measured at a scan rate of 10 mV/s under different disk rotation rates of 500, 900, 1200, 1600, and 2000 rpm. All the potentials in this study were reported with respect to the Ag/AgCl reference electrode.

In order to evaluate the time-drifting stability of the catalyst, current–time chronoamperometric responses of the catalysts and Pt/C were carried out in 0.1 M NaOH.

3. RESULTS AND DISCUSSION

The replication of ferrocene within the pores of SBA-15 mesoporous silica by carbonization under CVD conditions to generate CMK-5 mesoporous carbon with attractive structure of a 2-D hexagonally ordered carbon nanopipe was reported previously.[23] As shown in Scheme 1, first, the channel walls of SBA-15 mesoporous silica were coated with a thin film of CVD type Fe-containing carbon via a surface-templated process. The use of ferrocene as carbon precursor promotes the formation of graphitic carbon at mild conditions because of the metal-assisted catalytic graphitization. Second, during the in situ heteroatomic doping, Fe metal might help to anchor the sulfur and nitrogen atoms within the OMC framework, generating ORR active catalytic sites, though they still remain unknown.[11] We chose thiophene and pyrimidine as S and N precursors for heteroatomic doping owing to their low molecular weight and high S/C and N/C ratios (0.25 and 0.5, respectively), which is expected to reduce the pore clogging during the pyrolysis of CS and CN species and improve the doping levels, especially the nitrogen content. Finally, the metal and SBA-15 silica were etched away to obtain sulfur- and nitrogen-doped ordered mesoporous carbons (SN-OMCs).

The structures and morphologies of the as-synthesized SN-OMCs were characterized by SEM and TEM measurement. SEM images in Figure 1a revealed that the typical SN-OMC (SN-OMC-4) retains uniform rod-like morphology of the SBA-15 template, with average length and thickness of about 1 μm and 0.5 μm, respectively. These short rods join one after another to form lotus-root-like joints. Unlike the oligoporous nanoparticles (SN-C) prepared in the case of template-free CVD conditions (see the TEM image in Figure S1), the typical SN-OMC-4 demonstrates textural bimodal nanopores within the carbon framework along the [100] direction, as can be seen in the TEM image (Figure 1b; see the enlarged region A). The corresponding fast Fourier transforms of the patterns are shown in the inset. Similar mesostructures were also observed in TEM images for template-synthesized OMC, mono-doped S-OMC, N-OMC, as well as other SN-OMCs, as given in Figure S2. The surface textures of the SN-OMCs were characterized by N_2-sorption measurement. The isotherms and pore size distribution (PSD) of the SN-OMC-4 are shown in Figure 1c. The isotherm is of type IV with distinct H1 hysteresis loop

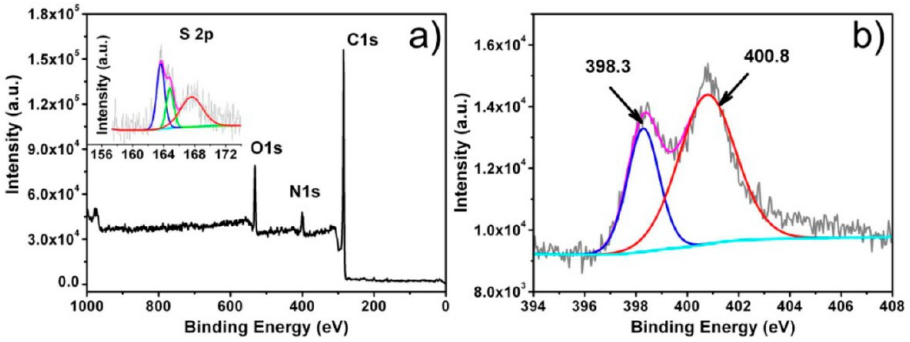

Figure 2. (a) XPS survey spectrum of SN-OMC-4 (inset shows the corresponding S2p spectrum) and (b) high-resolution N1s spectrum.

characteristics, indicating mesoporous characteristics including capillary condensation. The PSD was derived to be two overlapped peaks centered at ~3.5 and ~2.5 nm from desorption branch analysis using the Barrett–Joyner–Halenda method. Prolonging the CVD growth of OMC for enough time (16 h) led to the disappearance of the pore diameter (PD) centered at ~2.5 nm (see the PD for SN-OMC-16 in Table S1). This indicates the complete filling of the inner space of carbon nanopipes. Therefore, it could be concluded that the inner diameter of carbon nanopipes in the SN-OMC-4 is ~2.5 nm, and the pore centered at ~3.5 nm is generated from the trigonal channels after removal of the SBA-15 template. BET analysis upon the N_2-sorption isotherms (Figure S3) confirmed the large surface area of the template-synthesized samples, as listed in Table S1. Especially, the SN-OMC-4 possesses a maximum BET specific surface area of 1100 m^2 g^{-1}, nearly 2 times that of S,N-co-doped few-layered graphene oxide in our recent report,[18] and the corresponding total pore volume reaches ~0.83 cm^3 g^{-1}. The ordered mesoporous structure of the SN-OMC-4 was also confirmed by SAXS measurement. As shown in Figure 1d, the SAXS patterns showed four typical diffraction peaks which can be indexed to the (100), (110), (200), and (210) reflections of the 2-D hexagonal space group *P6mm* according to the theoretical simulation.[24] This result suggests that the SN-OMC-4 is indeed the surface replica from the SBA-15 template. The calculated cell parameter is a = 10.6 nm and slightly smaller than the value of 11.6 nm for the SBA-15 template (not shown), indicating a slight shrinkage after template elimination. In combination with the above bimodal PSD results, it can be concluded that the OMC framework retains CMK-5 structures with heteroatomic doping of sulfur and nitrogen.

The composition and the S and N moieties was examined by XPS, which are displayed in Figure 2 and Supporting Information Figures S4 and S5 and Table S1. The XPS survey spectrum for SN-OMC-4 (Figure 2a) shows considerable signals attributable to C1s, N1s, and O1s. The high-resolution S2p XPS spectrum in the inset of Figure 2a can be fitted to three energy components centered at around 163.6, 164.8, and 167.7 eV, corresponding to $S2p_{3/2}$, $S2p_{1/2}$, and S–O, respectively, which is in accordance with previous reports.[17,19] The XPS N1s spectra in Figure 2b reveal the incorporated N moieties to be pyridinic (398.3 eV) and pyrrolic/graphitic (400.8 eV).[18] Among the chemically bonded C, N, O, and S atoms, the C content of the SN-OMC-4 (86.3 %) dominates over N (4.7 %), O (8.3 %), and S (0.68 %). The levels of N and S in the SN-OMC-4 were both reduced with respect to those of mono-doped samples (6.2 atom % in N-OMC and 1.0 atom % in S-OMC, as shown in Table S1), similar to our previous findings.[18] From the elemental mapping of SN-OMC-4, the presence of the elements C, N, S, O (Figure 3a,b) and trace of

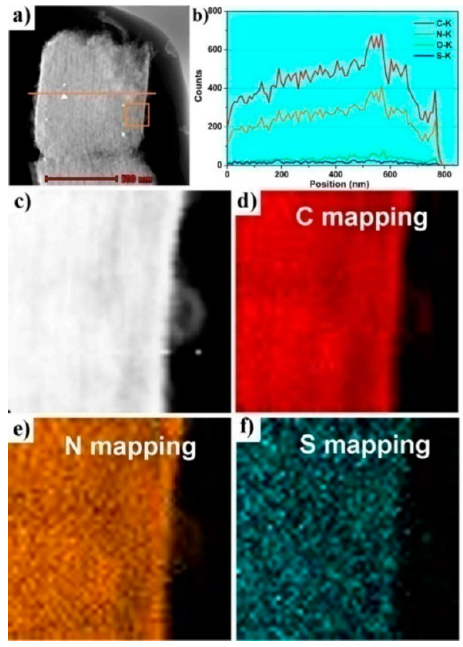

Figure 3. (a) Typical scanning transmission electron microscopy (STEM) image and (c) selected area STEM image of SN-OMC-4 (orange rectangle in (a)); (b) line mapping and (d–f) area mapping of C, N, and S, indicating the homogeneous dispersion of sulfur and nitrogen in the matrix framework of the SN-OMC-4.

Fe (not shown) was observed. Given the uniform distribution of C, N, and S within the CMK-5 carbon matrix (Figure 3c–f), we postulate that the inner walls of carbon nanopipes contain both N and S atoms.

To assess the ORR electrocatalytic activity of the SN-OMCs, CV experiments were performed in a three-electrode cell in O_2-free and O_2-saturated solution with 0.1 M NaOH at a scan rate of 50 mV s^{-1}. The results were compared with those of commercial Pt/C catalyst (20 % Pt loading, from E-tek) (Figure 4). In O_2-free solution, the SN-OMC-4 shows featureless CVs within the ORR potential range (Figure 4A, short-dotted line). In contrast, when the electrolyte solution was saturated with O_2, the reduction current appeared as a well-defined ORR peak at −0.16 V, which is similar to the value of commercial Pt/C catalyst (−0.16 V) (Figure 4B), positively shifted by 190 mV in comparison with that of lately reported sulfur–nitrogen co-doped carbon nanotubes (SN-CNTs)

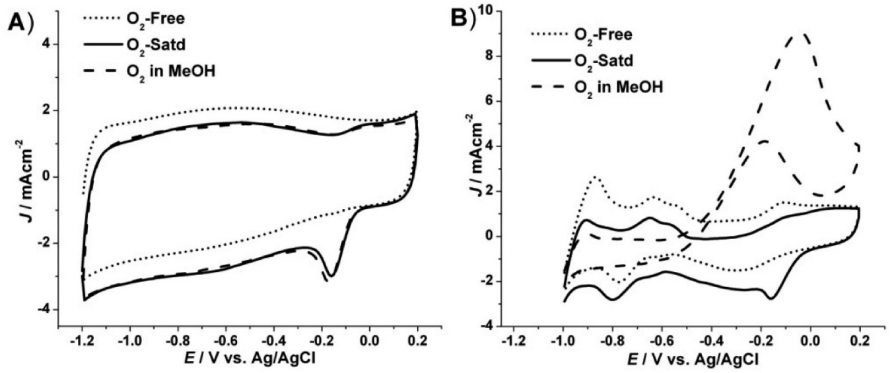

Figure 4. CV curves of (A) SN-OMC-4 and (B) commercial Pt/C electrodes in N_2- and O_2-saturated 0.1 M NaOH aqueous solution at a scan rate of 50 mV s^{-1}. The methanol tolerance was also evaluated upon addition of methanol (1 M).

(−0.35 V),[25] 100 mV positively shifted compared to that of nitrogen-doped ordered mesoporous graphitic array,[21] or 40 mV positively shifted as compared to sulfur−nitrogen co-doped three-dimensional carbon foams.[22] Such excellent catalytic ability of the synthesized SN-OMC-4 for ORR is probably due to the mesoporous carbon framework that is capable of providing large amounts of chemically active surface upon substitutional heteroatomic doping.[20] It is well-known that methanol can penetrate through the proton exchange membrane and deteriorate the cathode Pt catalyst, which is a major concern for a direct methanol fuel cell. To examine a possible methanol crossover effect, we also recorded CVs in O_2-saturated 0.1 M NaOH in the presence of 1.0 M methanol upon SN-OMC-4 and the commercial Pt/C catalyst. For the commercial Pt/C catalyst, a very strong pair of peaks at −0.18 and −0.05 V was observed, indicating methanol oxidation in the CV curve, whereas the cathodic ORR peak vanished (Figure 4B). In contrast, no noticeable change was observed on Pt-free SN-OMC-4 under the same conditions, similar to Pt-free, N-doped carbon materials.[8] All these suggest that the mesoporous SN-OMC-4 exhibits efficient ORR electrocatalytic activity with an excellent selectivity for oxygen electroreduction against methanol electro-oxidation. Therefore, it demonstrates a potential substitution to the high-cost Pt/C catalyst.

To get deeper insight into the electrochemical ORR process of the SN-OMC-4, linear sweep voltammograms (LSVs) on a rotating disc electrode (RDE) were recorded at different rotating speeds from 500 to 2000 rpm in 0.1 M NaOH electrolyte saturated with O_2. Analogous LSV curves were obtained for undoped OMC, mono-doped S-OMC, and N-OMC, as well as for commercial 20 wt % Pt/C catalyst for comparison. Typically, the LSV profiles of the SN-OMC-4 showed that current density was enhanced with increasing rotation rates (from 500 to 2000 rpm, Figure 5a). The SN-OMC-4 electrode displayed a very high ORR onset potential of approximately −0.05 V, which is very close to the value of −0.04 V for commercial 20 wt % Pt/C catalyst) and more positive than that of OMC (ca. −0.18 V), S-OMC (ca. −0.14 V), or N-OMC (ca. −0.075 V) at 1600 rpm (Figure 5b and the inset). Overall, heteroatomic doping leads to improvement of the ORR performance. Among the carbon catalysts, the most positive onset potential as well as highest reaction current on SN-OMC-4 indicates that dual-doped material has better catalytic performance than other carbon samples and also supports the proposed synergistic effect caused by dual N and S doping.[17,18] Moreover, between the single-doped samples, the onset potential of the N-OMC electrode (ca. −0.075 V) is much more positive than that of S-OMC (ca. −0.14 V). The diffusion current density from N-OMC is also much higher than that of the S-OMC electrode. Thus, with respect to the S-OMC electrode, the N-OMC showed much better electrocatalytic activity towards ORR. This was ascribed to the different doping configurations between N and S[19] and the higher doping level of N than S (see Table S1). Therefore, in a multi-doped carbon catalyst, the enhancement of ORR activity predominantly comes from doped nitrogen atoms. When comparing the LSV profiles of SN-OMC-4 to that of N-OMC, it is found that the dual-doped sample showed slightly positive shifts of half-wave potential ($\Delta E_{1/2}$ = 15 mV) and onset potential (ΔE_{onset} = 25 mV) for ORR.

The Koutecky−Levich (K−L) plots were obtained for each sample from the reaction current at −0.3 V on the LSVs at various rotating speeds (Figure 5a) to qualify the ORR process on these novel catalysts. The K−L plots for the SN-OMC-4 were also obtained at other potentials (Figure 5c). All the K−L plots exhibit good linearity over the potential range from −0.3 to −0.5 V (Figure 5c), implying that the reactions were first-order in the potential range.[18] The slopes remain approximately constant, which are more parallel to that of the theoretical four-electron pathway, indicating that O_2 electroreduction over the SN-OMC-4 electrode within the potential range tends to follow a four-electron transfer process. It is known that the limiting diffusion current density (J_L) depends on the rotation speed (ω) of the RDE, and therefore by using the K−L equation on this relationship, the limited kinetics current density (J_k) and the number of electron transfers (n) involved in the ORR can be calculated.[18,26] Details of the calculation method are provided in Supporting Information. For the SN-OMC-4 electrode, the exact electron transfer number at −0.3 V is 4.0, which is the same value as Pt/C (n = 4.0) and higher than that of N-OMC (n = 3.8), indicating a full four-electron pathway for ORR on SN-OMC-4, as was confirmed by the corresponding value of ∼3.9 calculated from rotating disk-ring electrode measurement (Figure S6). This value of n is also higher than the counterparts of the S and N dual-doped mesoporous graphene and few-layered graphene oxide (∼3.6−3.7);[17,18] the corresponding J_k value for the SN-OMC-4 sample (30.3 mA cm^{-2} at −0.3 V) is comparable to that of commercial Pt/C (33.4 mA cm^{-2} at -0.3 V, Figure 5d) and superior to that of N-OMC (26.0 mA cm^{-2}), S-OMC (14.2 mA cm^{-2}), and OMC catalyst (5.4 mA cm^{-2}), as ploted in Figure 5d. All these suggest that the ORR performance of co-doped carbon catalyst was

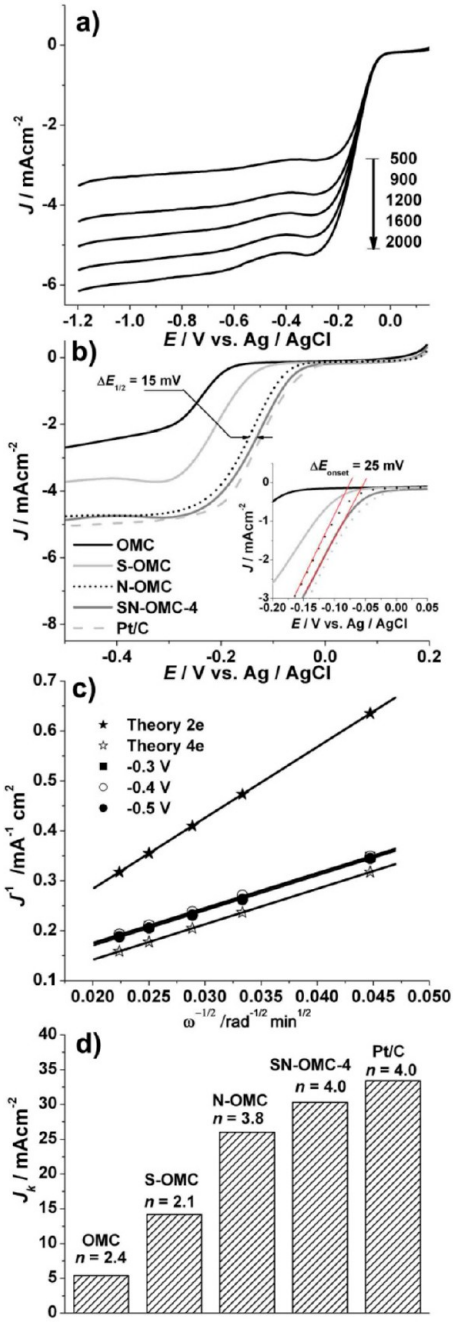

Figure 5. (a) RDE voltammograms for SN-OMC-4 supported on a GCE in O_2-saturated 0.1 M NaOH solution at a scan rate of 10 mV s^{-1} and various rotation rates. (b) RDE voltammograms of the undoped OMC, mono-doped S-OMC, N-OMC, double-doped SN-OMC-4, and commercial Pt/C supported on GCEs at a rotation rate of 1600 rpm. (c) Koutecky–Levich plot of J^{-1} versus $\omega^{-1/2}$ at different electrode potentials; the lines represent linear regression. (d) Electrochemical activity given for the kinetically limited current density (J_k) of different samples as well as the corresponding electron transfer numbers at −0.3 V.

enhanced upon additional S doping. As mentioned above, XPS revealed that the content of S in SN-OMC-4 is 0.68 atom %, while the N content decreased from 6.2 to 4.7 atom % after adding S. The low content of S in SN-OMC-4 suggests that it is difficult to dope sulfur with high content. Similarly, the recently reported sulfur and nitrogen co-doped carbon nanotube (SN-CNT) processed only 0.18 atom % S, which proved to be enough to further enhance ORR activity of SN-CNT with similar specific surface areas.[25] In our present SN-OMC-4 sample, the enhancement of ORR activity was expected to be contributed from doped S atoms (0.68 atom %), although the contribution to enhanced ORR activity from the increased surface area cannot be excluded (the BET surface area increased from 556 m^2/g for N-OMC to 1100 m^2/g for SN-OMC-4; see Table S1).

Optimal CVD conditions for the growth of the OMC framework is key to the high activity of the SN-OMCs for ORR. Besides SN-OMC-4, two additional SN-OMC samples were prepared by adjusting the deposition time of CVD of ferrocene for 20 min and 8 h. The two carbon catalysts were also tested on RDE to evaluate the ORR electrocatalytic activities in comparison with those of the oligoporous SN-C electrode prepared without a silica template.The template-free-synthesized oligoporous SN-C exhibits an inefficient two-step ORR process with onset potentials at -0.28 V and -0.70 V (Figure 6a), which can be attributable to reduction of O_2 to HO_2^- and HO_2^- to OH^-, respectively.[27] Unlike the oligoporous SN-C, the SN-OMCs showed almost only one current plateau with more positive onset potential (E_{onset}) and half-wave potentials ($E_{1/2}$). The growth of the OMC framework by controlling the CVD deposition time considerably influences the ORR activities of the final product. With prolonged OMC growth for 1/3, 4, and 8 h, the E_{onset} is tunable from −90 to −50 and −70 mV, while the $E_{1/2}$ is from −172 to −133 and −150 mV (Table 1). The SN-OMC-4 electrode exhibits the most positive onset and half-wave potential of −50 and −133 mV, very close to the values of commercial Pt/C catalyst of −40 and −120 mV, respectively (Figure 5b, Table 1). Moreover, for all SN-OMCs, the K–L plots derived from their polarization curves (Figure 5a and Figure S7) show linear graphs (Figure 5c and Figure S8). Based on the linear K–L plots, the J_k values and electron transfer numbers (n) were calculated (Figure 6b). Without the template, the as-prepared oligoporous SN-C exhibits poor ORR electrocatalytic activity, with J_k value and electron transfer number (n) at −0.4 V equal to 2.4 mA cm^{-2} and 2.3, respectively (see Figure 6b). Template fabrication significantly improves the ORR performance of doped carbon materials since the limited kinetics current density, J_k, and the electron transfer number, n, increased. Among the mesoporous SN-OMCs electrodes, a "volcanic" electrochemical activity appeared, where the J_k value at −0.3 V is tunable from 26.1 to 30.3 and 13.9 mA cm^{-2}, while the corresponding electron transfer number, n, is from 3.1 to ∼4.0 and 3.9. This indicates the intermediate ferrocene-derived mesoporous carbon framework plays a key role in determining the electrocatalytic activity of doped carbon materials. In combination with the surface texture parameters and chemical features of the SN-OMCs (Table 1), their ORR performance could be potentially understood. For example, the E_{onset} of the SN-OMCs is tunable from −90 to −50 and −70 mV, while the $E_{1/2}$ is from −172 to −133 and −150 mV, following the orders consistent with the levels of S content, implying the role of co-dopant S in reducing overpotential for ORR (Figure 5b), which is also in accordance with our previous report.[18] On the other hand, enhancing N-doping levels is a generally accepted strategy to improve the ORR efficiency of the NPMC.[19,28,29] However, the SN-OMC-8 with the highest total N content (8 atom %, both 2.8 atom % pyridinic-N and 5.2 atom % pyrrolic/graphitic-N) among the SN-OMC samples exhibits the smallest ORR electrocatalytic activity in terms of the limited kinetic

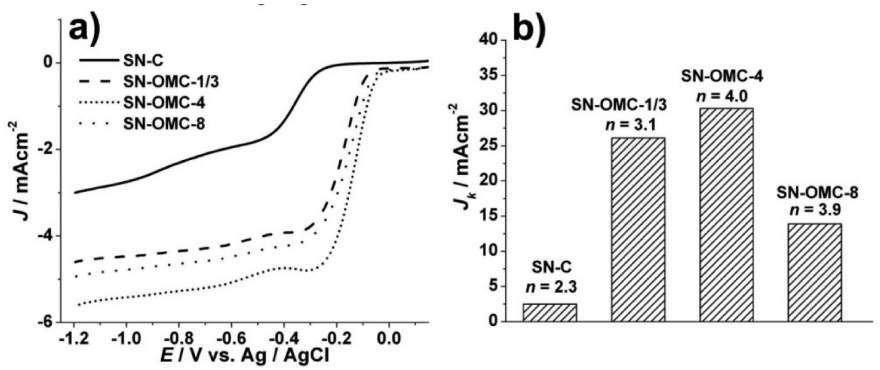

Figure 6. (a) RDE voltammograms of the oligoporous SN-C and double-doped SN-OMCs prepared at different CVD conditions supported on GCEs at a rotation rate of 1600 rpm and (b) kinetic-limited current density (J_k) at −0.3 V for different samples supported on GCEs as well as the corresponding electron transfer numbers at −0.3 V.

Table 1. Physicochemical Properties and the Electrocatalytic Activity of the SN-OMC Samples for ORR in Comparison with the Commercial Pt/C Catalyst

						atom %[e] N				
catalysts	CVD time[a] (h)	SA[b] (m^2 g^{-1})	PV[c] (cm^3 g^{-1})	PD[d] (nm)	atom %[e] S	$N-1$[f]	$N-2$[g]	$E_{onset}/E_{1/2}$[h] (mV/mV)	J_k[i] (mA cm^{-2})	n[j]
SN-OMC-1/3	1/3	750	0.53	3.4/2.2	0.25	2.1	3.2	−90/−172	26.1	3.1
SN-OMC-4	4	1100	0.83	3.5/2.5	0.68	2.4	2.3	−50/−133	30.3	4.0
SN-OMC-8	8	860	0.67	3.4/2.5	0.32	2.8	5.2	−70/−150	13.9	3.9
Pt/C								−40/−120	33.4	4.0

[a]Deposition time of OMC growth with ferrocene. [b]Specific surface area from multiple BET methods. [c]Total pore volume at $P/P_0 = 0.99$. [d]Average pore diameter, estimated using the desorption branch of the isotherm and the Barrett−Joyner−Halenda formula. [e]Atomic ratio data from XPS analyses. [f]Pyridinic-N at ∼398.3 eV. [g]Pyrrolic-/graphitic-N at ∼400−402 eV. [h]Onset potential (E_{onset}) and half-wave potential ($E_{1/2}$), estimated LSV measurement curves. [i]Kinetically limiting diffusion current density at −0.3 V. [j]Number of electron transfer.

current density (J_k = 13.9 mA cm^{-2}). The best ORR performance appeared on the SN-OMC-4 sample, which possesses the largest surface area (∼ 1100 m^2/g) and pore volume (∼0.83 cm^3/g) but contains intermediate N-doing level (4.7 atom %). These suggest that, in the SN-OMC electrocatalysts, the texture characteristic factor has superseded the chemically bonded dopants to be the key factor in controlling the ORR performance.

Since the optimized SN-OMC electrocatalyst demonstrated potential as a substitute for the commercial Pt/C electrode, we further tested the time-drift stability for the ORR. As shown in Figure 7, a continuous O_2 reduction (30 000 s) at −0.15 V (vs Ag/AgCl) on the SN-OMC-4 electrode resulted in only 16% loss of current density before becoming constant. The corresponding current loss over the Pt/C electrode under the same conditions was as high as approximately 30%. Therefore, the sulfur and nitrogen dual-doped, ferrocene-derived OMC framework with electrochemically active sites is much more stable and could be a potential substitute for a commercial Pt/C catalyst when applied in methanol-based and alkaline fuel cells.

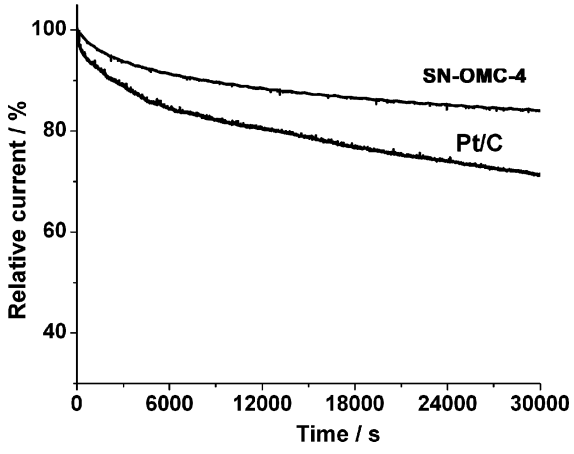

Figure 7. Time-drifting stability of the SN-OMC-4 and Pt/C at −0.15 V for 30 000 s with a rotation rate of 1600 rpm.

4. CONCLUSIONS

Sulfur- and nitrogen-doped ordered mesoporous carbons with large surface area, uniform bimodal pore systems have been fabricated by a templated method under CVD conditions. The ordered mesoporous carbons exhibited outstanding electrocatalytic activity, better stability, and higher methanol tolerance than the commercial Pt/C catalyst. Moreover, it is found that the textural mesostructure of the catalyst has superseded the chemically bonded dopants to be the key factor in controlling the ORR performance. In addition, our results also clarified the relationship between the textural mesostructure of metal-free carbon materials and the catalyst properties for ORR.

■ ASSOCIATED CONTENT

Supporting Information

Schematic drawing of CVD reaction system, details of characterizations including TEM, N_2 adsorption−desorption isotherms and XPS for composition and porous structure analysis of the SN-OMCs and the referred SN-C, OMC, S-OMC, N-OM samples; LSV tests for the comparison of their electrochemical activity. This material is available free of charge via the Internet at http://pubs.acs.org.

AUTHOR INFORMATION

Corresponding Author

*Tel: 86-591-83792835. Fax: 86-591-83792835. E-mail: guanlh@fjirsm.ac.cn.

Notes

The authors declare no competing financial interest.

ACKNOWLEDGMENTS

This work was financially supported by the National Natural Science Foundation of China (21101154, 21171163, and 91127020), the National Key Project on Basic Research (Grant No. 2011CB935904), and NSF for Distinguished Young Scholars of Fujian Province (Grant No. 2013J06006).

REFERENCES

(1) Darling, R. M.; Meyers, J. P. *J. Electrochem. Soc.* **2003**, *150*, 1523−1527.

(2) Wang, S. Y.; Iyyamperumal, E.; Roy, A.; Xue, Y. H.; Yu, D. S.; Dai, L. M. *Angew. Chem., Int. Ed.* **2011**, *50*, 11756−11760.

(3) Sun, Y. Q.; Li, C.; Xu, Y. X.; Bai, H.; Yao, Z. Y.; Shi, G. Q. *Chem. Commun.* **2010**, *46*, 4740−4742.

(4) Liang, Y. Y.; Li, Y. G.; Wang, H. L.; Zhou, J. G.; Wang, J.; Regier, T.; Dai, H. J. *Nat. Mater.* **2011**, *10*, 780−786.

(5) Huang, C. C.; Li, C.; Shi, G. Q. *Energy Environ. Sci.* **2012**, *5*, 8848−8868.

(6) Liang, J.; Zheng, Y.; Chen, J.; Liu, J.; Hulicova-Jurcakova, D.; Jaroniec, M.; Qiao, S. Z. *Angew. Chem., Int. Ed.* **2012**, *51*, 3892−3896.

(7) Wang, S. Y.; Zhang, L. P.; Xia, Z. H.; Roy, A.; Chang, D. W.; Baek, J. B.; Dai, L. M. *Angew. Chem., Int. Ed.* **2012**, *51*, 4209−4212.

(8) Gong, K. P.; Du, F.; Xia, Z. H.; Durstock, M.; Dai, L. M. *Science* **2009**, *323*, 760−764.

(9) Geng, D. S.; Chen, Y.; Chen, Y. G.; Li, Y. L.; Li, R. Y.; Sun, X. L.; Ye, S. Y.; Knights, S. *Energy Environ. Sci.* **2011**, *4*, 760−764.

(10) Yang, L. J.; Jiang, S. J.; Zhao, Y.; Zhu, L.; Chen, S.; Wang, X. Z.; Wu, Q.; Ma, J.; Ma, Y. W.; Hu, Z. *Angew. Chem., Int. Ed.* **2011**, *50*, 7132−7135.

(11) Lai, L. F.; Potts, J. R.; Zhan, D.; Wang, L.; Poh, C. K.; Tang, C. H.; Gong, H.; Shen, Z. X.; Jianyi, L. Y.; Ruoff, R. S. *Energy Environ. Sci.* **2012**, *5*, 7936−7942.

(12) Lee, J. S.; Park, G. S.; Kim, S. T.; Liu, M. L.; Cho, J. *Angew. Chem., Int. Ed.* **2013**, *52*, 1026−1030.

(13) Liu, Z. W.; Peng, F.; Wang, H. J.; Yu, H.; Zheng, W. X.; Yang, J. A. *Angew. Chem., Int. Ed.* **2011**, *50*, 3257−3261.

(14) Yang, Z.; Yao, Z.; Li, G. F.; Fang, G. Y.; Nie, H. G.; Liu, Z.; Zhou, X. M.; Chen, X.; Huang, S. M. *ACS Nano* **2012**, *6*, 205−211.

(15) Yao, Z.; Nie, H. G.; Yang, Z.; Zhou, X. M.; Liu, Z.; Huang, S. M. *Chem. Commun.* **2012**, *48*, 1027−1029.

(16) Yu, D. S.; Xue, Y. H.; Dai, L. M. *J. Phys. Chem. Lett.* **2012**, *3*, 2863−2870.

(17) Liang, J.; Jiao, Y.; Jaroniec, M.; Qiao, S. Z. *Angew. Chem., Int. Ed.* **2012**, *51*, 11496−11500.

(18) Xu, J. X.; Dong, G. F.; Jin, C. H.; Huang, M. H.; Guan, L. H. *ChemSusChem* **2013**, *6*, 493−499.

(19) Yang, S. B.; Zhi, L. J.; Tang, K.; Feng, X. L.; Maier, J.; Mullen, K. *Adv. Funct. Mater.* **2012**, *22*, 3634−3640.

(20) Zheng, Y.; Jiao, Y.; Chen, J.; Liu, J.; Liang, J.; Du, A.; Zhang, W. M.; Zhu, Z. H.; Smith, S. C.; Jaroniec, M.; Lu, G. Q.; Qiao, S. Z. *J. Am. Chem. Soc.* **2011**, *133*, 20116−20119.

(21) Liu, R. L.; Wu, D. Q.; Feng, X. L.; Mullen, K. *Angew. Chem., Int. Ed.* **2010**, *49*, 2565−2569.

(22) Liu, Z.; Nie, H. G.; Yang, Z.; Zhang, J.; Jin, Z. P.; Lu, Y. Q.; Xiao, Z. B.; Huang, S. M. *Nanoscale* **2013**, *5*, 3283−3288.

(23) Lei, Z. B.; Bai, S. Y.; Xiao, Y.; Dang, L. Q.; An, L. Z.; Zhang, G. N.; Xu, Q. *J. Phys. Chem. C* **2008**, *112*, 722−731.

(24) Schmidt, W. *Microporous Mesoporous Mater.* **2009**, *117*, 372−379.

(25) Shi, Q. Q.; Peng, F.; Liao, S. X.; Wang, H. J.; Yu, H.; Liu, Z. W.; Zhang, B. S.; Su, D. S. *J. Mater. Chem. A* **2013**, *1*, 14853−14857.

(26) Chen, W.; Chen, S. W. *Angew. Chem., Int. Ed.* **2009**, *48*, 4386−4389.

(27) Yang, D. S.; Bhattacharjya, D.; Inamdar, S.; Park, J.; Yu, J. S. *J. Am. Chem. Soc.* **2012**, *134*, 16127−16130.

(28) Wang, H. B.; Maiyalagan, T.; Wang, X. *ACS Catal.* **2012**, *2*, 781−794.

(29) Lin, Z. Y.; Waller, G.; Liu, Y.; Liu, M. L.; Wong, C. P. *Adv. Energy Mater.* **2012**, *2*, 884−888.